Università degli Studi di Padova

Dipartimento di Fisica e Astronomia "Galileo Galilei"

M.Sc. Degree in Physics

Physics Laboratory report

Measurement of Environmental Radiation

Vanessa Cerrone - 2053044

Sabrina Ciarlantini -2054770

Aurora Leso - 2055703

15/16/17 December 2021

Academic Year 2021/2022

1 Aims of the experiment

1. Obtaining the **best resolution** possible for both **HPGe and NaI(Tl)** detectors;
2. Finding the **energy and efficiency calibration** for the detectors used;
3. Measuring **environmental radioactivity** by using organic and inorganic materials;
4. Performing an **indoor radon measurement**.

2 Experimental setup

In this section, a description of the experimental setup is provided.

- **Shielded well**;
- **Detectors**: NaI(Tl) inorganic scintillator and HPGe (i.e. hyper-pure germanium) detector;
- **Photomultipliers** (PMTs);
- **Oscilloscope**: Tektronix TBS 1012B-EDU;
- **CAEN Digitizer**;
- **CAEN power module**;
- Some samples of both organic and inorganic materials and of known radionuclides;
- A sample of air humidity that was collected with a canister.

In order to estimate the energy, it's not possible to integrate the incoming signal because it is too large, hence it has to be reshaped with a trapezoidal filter. Additionally, to obtain the best energy resolution for both the HPGe and the NaI(Tl) detectors, the parameters shown in Table 1 were set:

- **Decay Time**: an estimate of the average decay time of the observed signals;
- **Trapezoid Rise Time**: the desired duration for the trapezoid shape rising;
- **Trapezoid Flat Top**: the desired time duration of the flat part on top of the trapezoid shape;
- **Trapezoid Rescaling**: a rescaling parameter that can be chosen in order to better observe the shape on the screen.

Parameter	NaI (ch0)	HPGe (ch1)
Threshold [a.u.]	200	100
Decay Time [a.u.]	10000	4000
Rise Time [a.u.]	500	300
Flat Top [a.u.]	300	100
Rescaling [a.u.]	11	20

Table 1: Trapezoidal filter settings.

3 Energy calibration

To calibrate the acquired spectra we have used the linear function reported below:

$$E[\text{keV}] = \alpha + \beta \cdot (\text{ADC counts})$$

The parameters and the regression plots obtained for NaI(Tl) and HPGe detectors are displayed in Table 2 and Figure 1, respectively.

	α [keV]	β [keV/ADC counts]
NaI(Tl)	-8.973 ± 0.002	0.0878 ± 0.0004
HPGe	-0.0192 ± 0.0001	0.14891 ± 0.00001

Table 2: Results of the linear regressions for the energy calibration.

where the expected peak energies have been taken from LNHB[1] website. Since the background before and after each peak appears variable, to fit the peaks a gaussian plus a linear background is used:

$$f(x) = a + b \cdot x + \mathrm{N} \cdot e^{-\frac{(x-\mu)^2}{2\sigma^2}} \tag{1}$$

[1]Laboratoire National Henri Becquerel, `http://www.lnhb.fr`

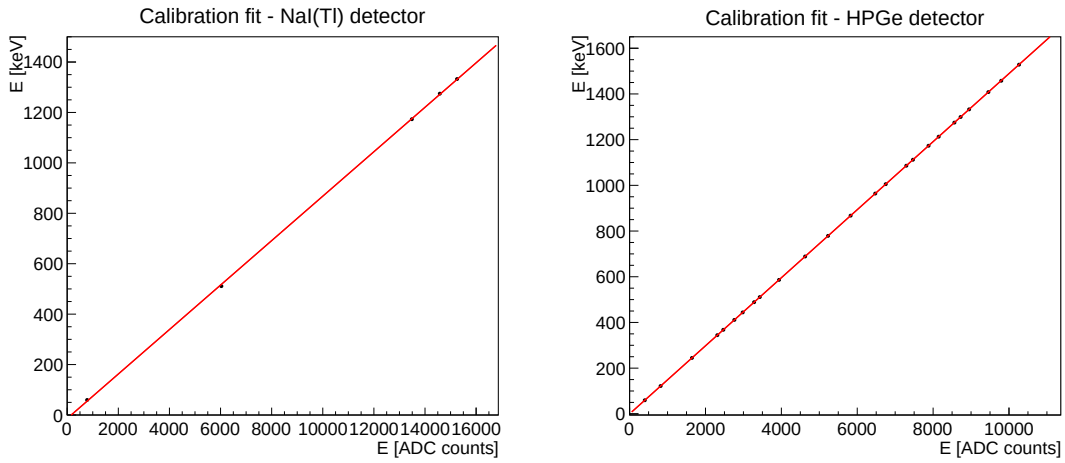

Figure 1: Calibration fit plots. On the left hand-side for NaI(Tl), on the right hand-side for HPGe.

The energy calibration fit was performed using the following sources: ^{241}Am, ^{60}Co and ^{22}Na for both detectors, plus ^{152}Eu only for the HPGe: the peaks resulting from the spectra of the last source mentioned cannot be distinguished one from another with the Na(Tl) detector due to its lower resolution. Some results of the gaussian fits are reported in Table 3 and Table 4.

NaI(Tl)				
Source	Expected Energy [keV]	μ [ADC counts]	σ [ADC counts]	R [%]
^{241}Am	59.5409(1)	780.2 ± 0.4	35.6 ± 0.5	14.5
^{60}Co	1173.228(3)	13486 ± 2	282 ± 2	4.3
^{60}Co	1332.492(4)	15253 ± 2	302 ± 3	4.1
^{22}Na	511	6032.8 ± 0.9	183 ± 1	7.0
^{22}Na	1274.537(7)	14581 ± 3	282 ± 5	4.8
HPGe				
Source	Expected Energy [keV]	μ [ADC counts]	σ [ADC counts]	R [%]
^{241}Am	59.5409(1)	400.034 ± 0.02	6.58 ± 0.01	3.8
^{60}Co	1173.228(3)	7879.43 ± 0.05	9.75 ± 0.05	0.3
^{60}Co	1332.492(4)	8949.36 ± 0.06	10.02 ± 0.05	0.2
^{22}Na	511	3431.27 ± 0.06	11.67 ± 0.07	0.7
^{22}Na	1274.537(7)	8560.62 ± 0.07	9.14 ± 0.07	0.2

Table 3: Energy calibration data: results of gaussian fit for non-calibrated spectra for both detectors.

Expected Energy [keV]	μ [keV]	σ [keV]	R [%]
121.7817(3)	121.684 ± 0.005	2.39 ± 0.01	2.0
244.6974(8)	244.61 ± 0.01	2.40 ± 0.03	1.0
344.279(1)	344.172 ± 0.007	2.52 ± 0.01	0.7
411.117(1)	411.05 ± 0.03	2.23 ± 0.08	0.5
443.965(3)	443.83 ± 0.03	2.52 ± 0.07	0.6
586.265(3)	586.4 ± 0.1	2.2 ± 0.4	0.4
688.670(5)	688.5 ± 0.1	3.1 ± 0.3	0.4
778.905(2)	778.82 ± 0.02	2.74 ± 0.03	0.3
867.380(3)	867.32 ± 0.04	2.67 ± 0.07	0.3
964.08(2)	964.00 ± 0.02	2.83 ± 0.03	0.3
1005.27(2)	1005 ± 1	2.7 ± 0.2	0.3
1085.84(1)	1085.923 ± 0.004	3.21 ± 0.05	0.3
1112.076(3)	1112.00 ± 0.02	2.88 ± 0.03	0.3
1212.95(1)	1212.93 ± 0.08	2.9 ± 0.1	0.2
1299.142(8)	1299.05 ± 0.07	3.0 ± 0.1	0.2
1408.013(3)	1407.97 ± 0.02	3.07 ± 0.03	0.2
1457.64(1)	1457.8 ± 0.1	3.5 ± 0.3	0.2
1528.10(2)	1528.2 ± 0.1	3.2 ± 0.3	0.2

Table 4: Energy calibration data for ^{152}Eu. The calibrated spectrum peaks are reported.

4 Efficiency of the detectors

4.1 Efficiency curve

In order to obtain the absolute efficiency curve of the detectors in function of the peak energies, the visible peaks of the different sources were fitted with a gaussian plus a linear background. Knowing the counts under the single photo-peaks, the intrinsic efficiency at different energies is computed with

the following formula:

$$\epsilon = \frac{\mathrm{N_{peak}}}{\mathrm{A} \cdot \mathrm{W} \cdot \epsilon_{\mathrm{g}} \cdot \Delta \mathrm{t}} \tag{2}$$

where

- $\mathrm{N_{peak}}$ is the photo peak area;
- A is the source activity (find reference to website of department;
- W is the weight of the transition, i.e. the number of photons per 100 disintegrations;
- ϵ_g is the geometric efficiency of the detector;
- Δt is the time duration of the data acquisition.

The geometric factor ϵ_{g} corresponds to the solid angle fraction covered by the detectors and can be defined as:

$$\epsilon_{\mathrm{g}} = \frac{\pi \mathrm{r}^2}{4\pi \mathrm{d}^2}$$

where r is the radius of the detector and d is the distance between the former and the source, reported in Table 5.

Detector	Radius r [cm]	Distance d [cm]	Geometric efficiency ϵ_{g}
NaI(Tl)	3.75	24	$(6.10 \pm 0.07) \cdot 10^{-3}$
HPGe	1.95	20	$(2.39 \pm 0.03) \cdot 10^{-3}$

Table 5: Geometric factors

First of all, we subtracted the background to the acquired spectra, using a proper normalization factor to account for the different acquisition times. After that, we integrated over each peak range, in order to get the number of events $\mathrm{N_{peak}}$. All the data acquisitions lasted 10 minutes, apart from the one for the ^{152}Eu source, which was 20 minutes long. The activities[2] of the sources are:

$$\mathrm{A}(^{241}\mathrm{Am}) = 421 \text{ kBq} \qquad \mathrm{A}(^{60}\mathrm{Co}) = 195 \text{ kBq} \qquad \mathrm{A}(^{22}\mathrm{Na}) = 110 \text{ kBq} \qquad \mathrm{A}(^{152}\mathrm{Eu}) = 84 \text{ kBq}$$

The quantities that are taken into account as a contribution to the total error of ϵ are the photo-peak area $\mathrm{N_{peak}}$, the branching ratio of the transition and ϵ_g. The first has been computed following the Poisson distribution while the third through propagation. For what regards the second one, we have used the uncertainty taken from the LNHB website. The total error of ϵ has thus been computed through propagation. The results are reported in Table 6 and Table 7, for the NaI(Tl) and HPGe detectors, respectively.

Source	Peak energy [keV]	$\mathrm{N_{peak}}$	W	Efficiency ϵ
^{241}Am	58.796 ± 0.008	$(327.1 \pm 0.6) \cdot 10^3$	0.3592(17)	0.591 ± 0.001
^{60}Co	1174.40 ± 0.09	$(152.4 \pm 0.4) \cdot 10^3$	0.9985(3)	0.2138 ± 0.0006
	1331.4 ± 0.1	$(92.2 \pm 0.3) \cdot 10^3$	0.999626(6)	0.1291 ± 0.0005
^{22}Na	520.20 ± 0.04	$(85.0 \pm 0.3) \cdot 10^3$	1.807(2)	0.1168 ± 0.0004
	1271.1 ± 0.1	$(40.6 \pm 0.2) \cdot 10^3$	0.9994(13)	0.1008 ± 0.0005

Table 6: Efficiency curve parameters for NaI(Tl) detector.

As one can see in Table 7, the ^{241}Am peak and the ^{152}Eu peak at energy $\sim$ 121 keV result with an efficiency > 1: these nonphysical results are probably due to the fact that the activity of the two involved sources is too high.

[2]Sorgenti Radiogene: Dipartimento di Fisica e Astronomia, "Polo Didattico" `https://www.dfa.unipd.it/fileadmin/servtec/Sorgenti_polo_sett_2021_01.pdf`

Additionally, in order to get relative values of peak efficiencies, the ^{152}Eu efficiency values obtained have all been renormalized so that the efficiency value of the 1408 keV peak of the same source results equal to 1 (see Figure 2).

Source	Peak energy [keV]	N_{peak}	W	Efficiency ϵ
^{241}Am	59.540 ± 0.003	$(251.91 \pm 0.02) \cdot 10^3$	0.3592(17)	1.163 ± 0.003
^{60}Co	1173.138 ± 0.007	$(43.8 \pm 0.2) \cdot 10^3$	0.9985(3)	0.1571 ± 0.0008
	1332.416 ± 0.007	$(39.6 \pm 0.2) \cdot 10^3$	0.999626(6)	0.1419 ± 0.0008
^{22}Na	510.807 ± 0.006	$(78.4 \pm 0.3) \cdot 10^3$	1.807(2)	0.275 ± 0.001
	1274.59 ± 0.01	$(19.9 \pm 0.1) \cdot 10^3$	0.9994(13)	0.1261 ± 0.0009
^{152}Eu	121.7817 ± 0.0003	$(69.3 \pm 0.3) \cdot 10^3$	0.2841(13)	1.014 ± 0.005
	244.6974 ± 0.0008	$(11.5 \pm 0.1) \cdot 10^3$	0.0755(4)	0.635 ± 0.008
	344.279 ± 0.001	$(30.5 \pm 0.2) \cdot 10^3$	0.2659(12)	0.477 ± 0.003
	411.117 ± 0.001	$(20.2 \pm 0.4) \cdot 10^2$	0.02238(1)	0.38 ± 0.01
	443.965 ± 0.003	$(28.3 \pm 0.5) \cdot 10^2$	0.028(2)	0.31 ± 0.02
	586.265 ± 0.003	$(3.5 \pm 0.2) \cdot 10^2$	0.00462(4)	0.27 ± 0.01
	688.670 ± 0.005	$(5.5 \pm 0.2) \cdot 10^2$	0.00841(6)	0.420 ± 0.009
	778.905 ± 0.002	$(72.3 \pm 0.9) \cdot 10^2$	0.1297(6)	0.232 ± 0.003
	867.380 ± 0.003	$(20.4 \pm 0.5) \cdot 10^2$	0.04243(23)	0.200 ± 0.005
	964.08 ± 0.02	$(64.5 \pm 0.8) \cdot 10^2$	0.145(6)	0.185 ± 0.002
	1005.27 ± 0.02	$(3.9 \pm 0.2) \cdot 10^2$	0.00665(23)	0.24 ± 0.01
	1085.84 ± 0.01	$(45.7 \pm 0.7) \cdot 10^2$	0.1013(6)	0.187 ± 0.003
	1112.076 ± 0.003	$(55.6 \pm 0.7) \cdot 10^2$	0.1341(6)	0.172 ± 0.003
	1212.95 ± 0.01	$(5.4 \pm 0.2) \cdot 10^2$	0.01416(9)	0.160 ± 0.007
	1299.142 ± 0.008	$(5.8 \pm 0.2) \cdot 10^2$	0.01633(9)	0.150 ± 0.007
	1408.013 ± 0.003	$(70.0 \pm 0.8) \cdot 10^2$	0.2085(8)	0.140 ± 0.002
	1457.64 ± 0.01	$(1.5 \pm 0.1) \cdot 10^2$	0.00498(4)	0.13 ± 0.01
	1528.10 ± 0.02	$(1.0 \pm 0.1) \cdot 10^2$	0.00281(5)	0.15 ± 0.02

Table 7: Efficiency curve parameters for HPGe detector.

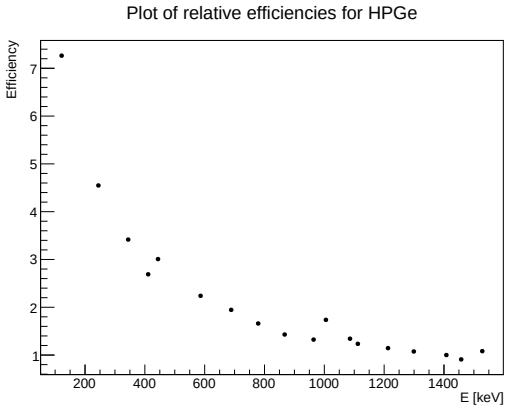

Figure 2: Relative efficiency plot for HPGe detector, for ^{152}Eu source peaks.

4.2 Efficiency fit

The efficiency fit used for the HPGe detector is [3]:

$$\epsilon = a_1[\exp(-a_2\ \mathrm{E}^{a_3}) + \exp(a_4\ \mathrm{E}^{a_5})] \cdot (1 - \exp(a_6\ \mathrm{E}^{a_7})) \tag{3}$$

[3]Expression taken from one of the models considered the most precise for germanium detectors up to now [Hurtado et Al., N.I.M. A 594 2008]

while for the NaI detector[4]:

$$\epsilon = \frac{a_1 \cdot \mathrm{E}^{a_2}}{1000 \cdot a_3 + \mathrm{E}^{a_4}} \tag{4}$$

The absolute efficiency curves for both detectors are depicted in Figure 3.

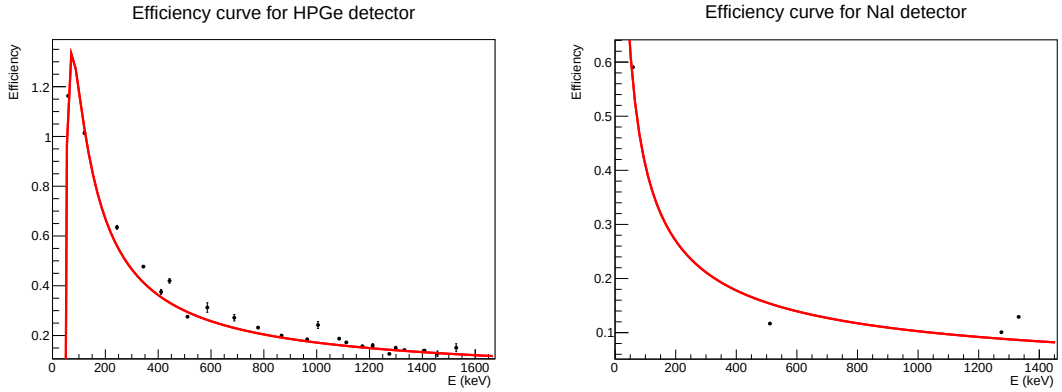

Figure 3: Efficiency fit: on the left, the result for HPGe detector; on the right the result for NaI(Tl) detector.

Concerning the HPGe detector, the 59 keV peak of the ^{241}Am has, in contrast with what is expected, an efficiency value higher than the 121 keV peak of ^{152}Eu. Since the fit function is quite complex (7 parameters), its shape can vary a lot according to both the initial parameters set and the points considered for the fit. As one can see in Figure 3, the curve well describes the data for high energies, but it needs to be underlined that this fit is not reliable for low energies, due to the absence of peaks (we have only the ^{241}Am peak, and the resulting value is unphysical), and to the more incisive contribution of the electronic setup in this region.
For what concerns the NaI(Tl) detector, according to the very restricted number of peaks considered, the fit cannot be considered reliable at any energy range.

5 Gamma decay for different samples

In this section different samples were analyzed using gamma-ray spectroscopy, with the purpose of identifying the presence of radionuclides and of measuring the activity of each source. Firstly, the background is subtracted from the sample spectra and the peaks of interest are fitted with a gaussian plus linear background fit. The activity, in [Bq/kg], associated to each transition is computed as follows:

$$A = \frac{\mathrm{N_{peak}}}{\Delta\mathrm{t} \cdot \mathrm{m} \cdot \epsilon \cdot \mathrm{W} \cdot \epsilon_g} \tag{5}$$

- $\mathrm{N_{peak}}$ is the area under the specific peak, obtained through the integral in the appropriated region;
- Δt is the acquisition time, which varies according to the analyzed sample;
- m is the mass of the sample;
- ϵ is the peak efficiency at different energies, computed by using the parameters obtained in Section 4.2;
- W is the branching ratio associated to the decay;
- ϵ_g is the geometric efficiency, defined in Section 4.1 and recalculated with the distances of the samples from the detectors in this configuration:

$$d_{\mathrm{NaI(Tl)}} \sim 2 \text{ cm} \implies \epsilon_g \sim 0.88 \qquad d_{\mathrm{HPGe}} \sim 10 \text{ cm} \implies \epsilon_g \sim 0.95 \cdot 10^{-2}$$

Since the samples were positioned at a small distance from the detectors, the uncertainties of the solid angles are large and difficult to be properly evaluated; as a consequence they significantly affect the accuracy of the activity measurements.

[4]One of the most used functions for NaI detectors, taken from Kalfas et al., 2016

Sample	KCl	Mushrooms	Bricks	ZrO_2	Electrodes	Porphyry	Autunite
Weight [g]	8	16.6	120.4	1870	92.5	502.3	29
Δt [min]	30	15	8	21	16	41	30

Table 8: Weight and acquistion time for the different samples.

Table 22 in the Appendix shows a comprehensive list of the most intense peaks that were identified and fitted in the spectra presented in Figures 3-8, with the theoretical energy value and branching ratio, the corresponding isotope[4] and the activity of the source associated to the specific gamma emission.

Potassium Chloride A potassium chloride (KCl) sample is used to determine the activity of the radioactive isotope ^{40}K, contained in small quantities in natural potassium. 90% of ^{40}K undergoes a β transition into the ground state of ^{40}Ca,, whereas the remaining 10% decays into an excited state of ^{40}Ar, that emits a 1460.82 keV gamma-ray in the transition to the ground state. In the acquired spectra in Figure 4 the peak of interest is found and identified with good accuracy. The total activity of the sample is obtained using Equation 5:

$$A_{NaI(Tl)} = (7.9 \pm 0.3) \cdot 10^3 \text{ Bq/kg} \qquad A_{HPGe} = (5.9 \pm 0.6) \cdot 10^4 \text{ Bq/kg}$$

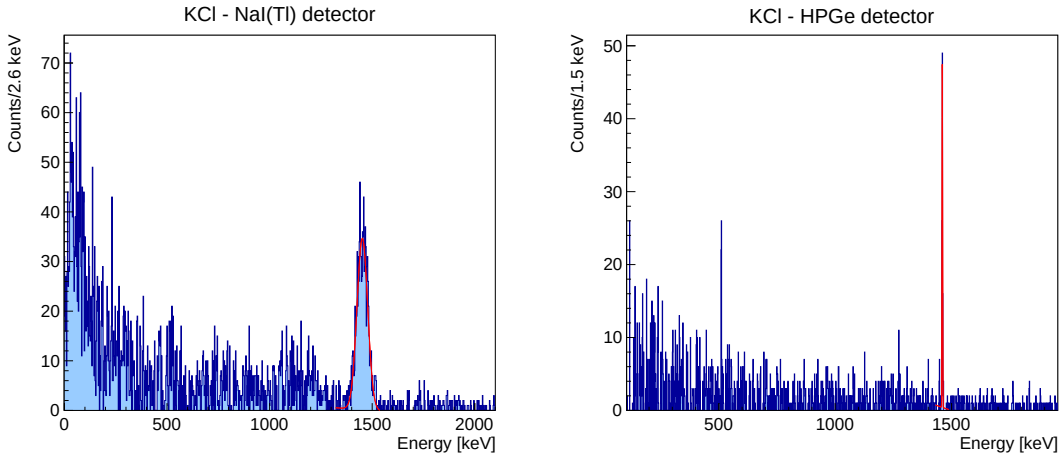

Figure 4: KCl spectra

Mushrooms A sample of spontaneous mushrooms is analyzed in order to evaluate the concentration of the artificial radioactive isotope Caesium-137, mainly released into the environment after nuclear accidents. Its presence is indicated by the characteristic 662 keV peak, which is clearly identifiable only in the NaI(Tl) spectrum (left panel of Figure 5). The total activity of this sample is estimated:

$$A_{NaI(Tl)} = (66 \pm 6) \text{ Bq/kg}$$

[4]In all tables the parent nucleus is indicated, but it needs to be underlined that the identified γ rays are emitted by the daughter nucleus in an excited state.

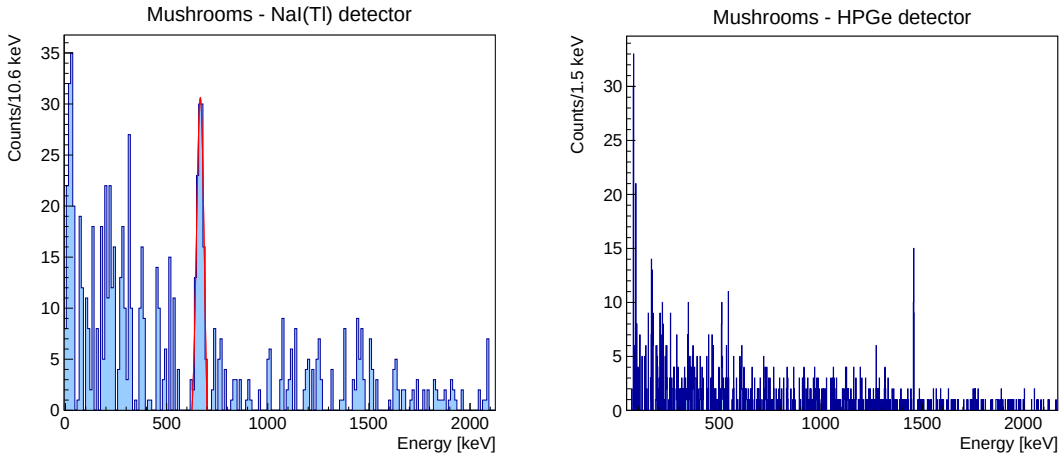

Figure 5: Mushrooms spectra

Zirconium Oxide Zirconium Oxide (ZrO_2) typically contains trace amounts of radionuclides such as radium, thorium, and uranium. Products of the ^{232}Th chain are found, such as ^{208}Tl and ^{228}Ac, together with others that come from the radioactive series[5] of ^{226}Ra, i.e. ^{214}Pb and ^{214}Bi. The corresponding activities are calculated and reported in Table 9 and Table 10, whereas the acquired spectra are shown in Figure 6. The gamma spectrum of a radium source exhibits many lines but the peak at 186 keV is the only one that comes directly from the Radium-226 decay, namely from an excited state of Radon-222.

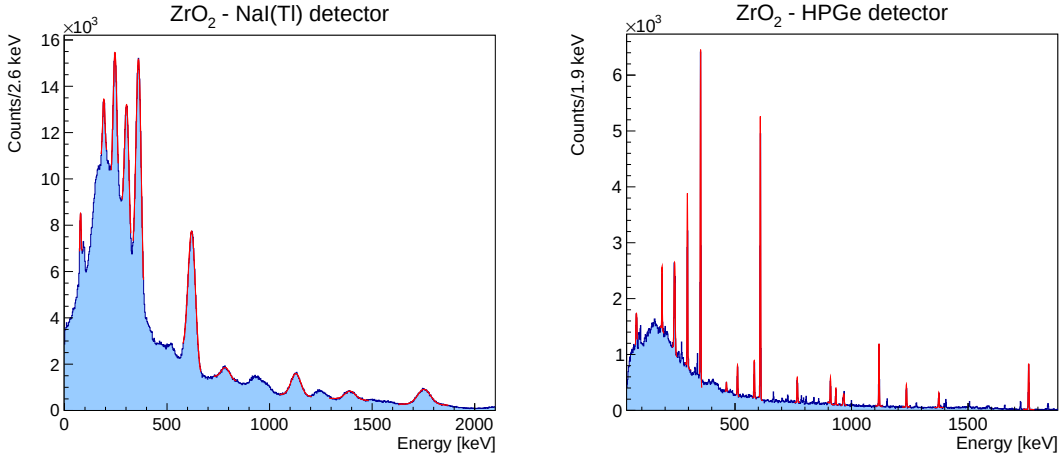

Figure 6: ZrO_2 spectra for both detectors.

NaI(Tl)	
Isotope	Activity [Bq/kg]
^{214}Pb	$(34.1 \pm 0.3) \cdot 10^3$
^{214}Bi	$(115.0 \pm 0.2) \cdot 10^2$
^{226}Ra	$(60.5 \pm 0.2) \cdot 10^2$

Table 9: ZrO_2 sample results for NaI(Tl) detector.

HPGe	
Isotope	Activity [Bq/kg]
^{214}Pb	$(409.1 \pm 0.8) \cdot 10^2$
^{214}Bi	$(13.7 \pm 0.1) \cdot 10^4$
^{226}Ra	$(31.0 \pm 0.1) \cdot 10^3$
^{228}Ac	$(7.1 \pm 0.2) \cdot 10^3$
^{208}Tl	$(3.5 \pm 0.3) \cdot 10^2$

Table 10: ZrO_2 sample results for HPGe detector.

2% Thoriated electrodes In this sample, we expect to find elements that are present in the decay chain of Thorium-232, which accounts for nearly all natural thorium in nature. The acquired spectra

[5]Radium-226 itself is part of the ^{238}U chain.

are reported in Figure 7; the higher resolution of the HPGe detector allows to identify a larger amount of transitions, yet the main peaks are visible in both spectra. Indeed, we can identify the main photopeak at 239 keV, generated by ^{212}Pb. The main other isotopes that are identifiable in the gamma spectrum are ^{212}Bi, ^{208}Tl and ^{228}Ac (e.g., peaks at 727 keV, 583 keV and 911 keV, respectively). Since the 50-120 keV region includes lines from X-ray emissions, the intensities were not estimated. The activity of each radionuclide is estimated by summing over all the associated events and it's reported in Table 11 and Table 12.

NaI(Tl)	
Isotope	Activity [Bq/kg]
^{212}Pb	$(21.2 \pm 0.2) \cdot 10^3$
^{212}Bi	$(74.1 \pm 0.4) \cdot 10^3$
^{228}Ac	$(21.7 \pm 0.6) \cdot 10^4$
^{208}Tl	$(40.8 \pm 0.3) \cdot 10^3$

Table 11: Electrodes sample results for NaI(Tl) detector.

HPGe	
Isotope	Activity [Bq/kg]
^{212}Pb	$(3.2 \pm 0.1) \cdot 10^5$
^{212}Bi	$(129.7 \pm 0.8) \cdot 10^3$
^{228}Ac	$(7.1 \pm 0.2) \cdot 10^5$
^{208}Tl	$(1.1 \pm 0.7) \cdot 10^3$

Table 12: Electrodes sample results for HPGe detector.

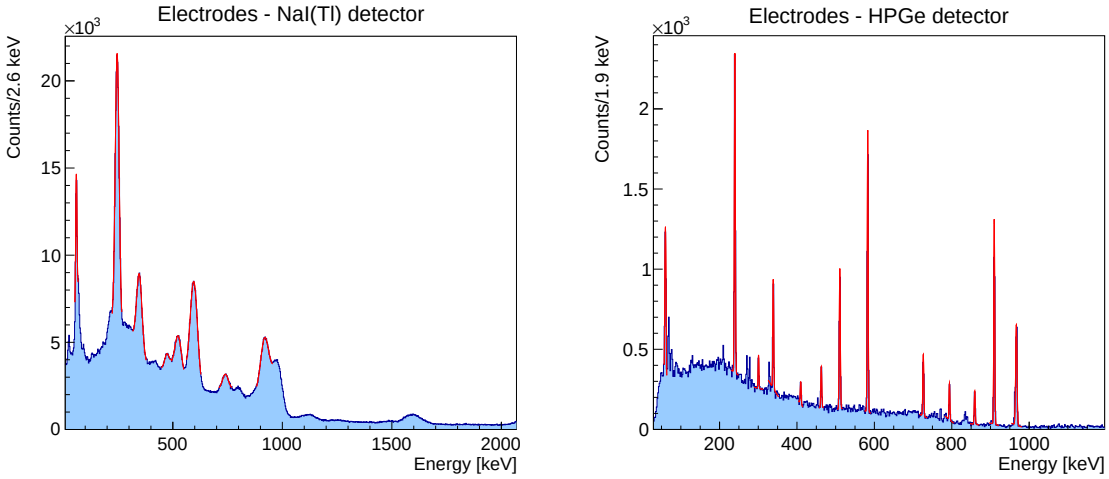

Figure 7: Thoriated electrodes spectra

Porphyry Porphyry is an igneous rock that contains small amounts of radioactive elements, namely deriving from the ^{226}Ra and ^{232}Th series and from ^{40}K. Indeed, we identified peaks associated to the aforementioned isotopes and the resulting activity for each one of them is reported in Table 13 and Table 14.

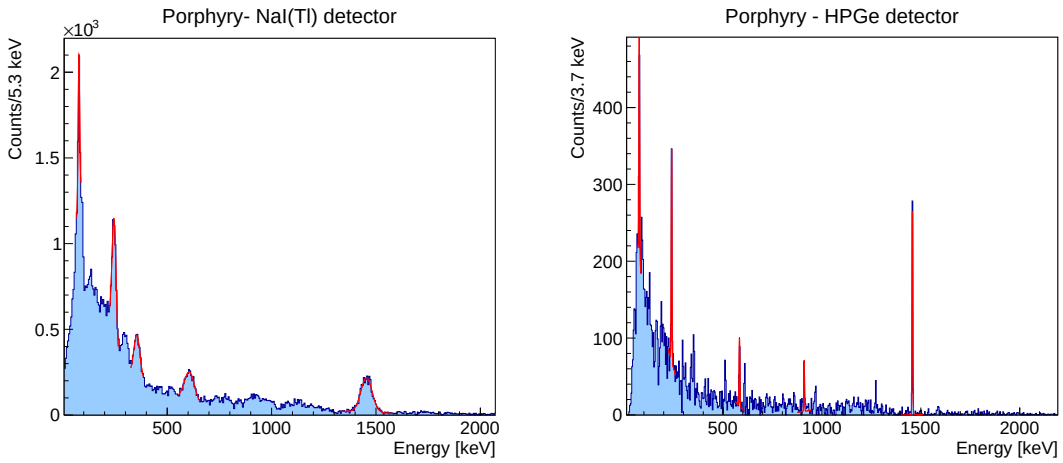

Figure 8: Porphyry spectra

NaI(Tl)	
Isotope	Activity [Bq/kg]
^{214}Pb	120.0 ± 0.3
^{212}Pb	58.1 ± 0.7
^{228}Ac	$(17.1 \pm 0.6) \cdot 10$
^{208}Tl	26.6 ± 0.4
^{40}K	$(35.6 \pm 0.4) \cdot 10$

Table 13: Porphyry sample results for NaI(Tl) detector.

HPGe	
Isotope	Activity [Bq/kg]
^{214}Pb	$(79.6 \pm 0.3) \cdot 10$
^{212}Pb	$(36.2 \pm 0.6) \cdot 10$
^{228}Ac	$(3.2 \pm 0.1) \cdot 10^2$
^{208}Tl	$(6.3 \pm 0.3) \cdot 10$
^{40}K	$(21.2 \pm 0.3) \cdot 10^2$

Table 14: Porphyry sample results for HPGe detector.

Autunite Autunite is a mineral that features a moderate uranium content. In the gamma spectra in Figure 9, peaks of ^{226}Ra and its descendants ^{214}Pb and ^{214}Bi are visible. The corresponding activity can be found in Table 15 and Table 16.

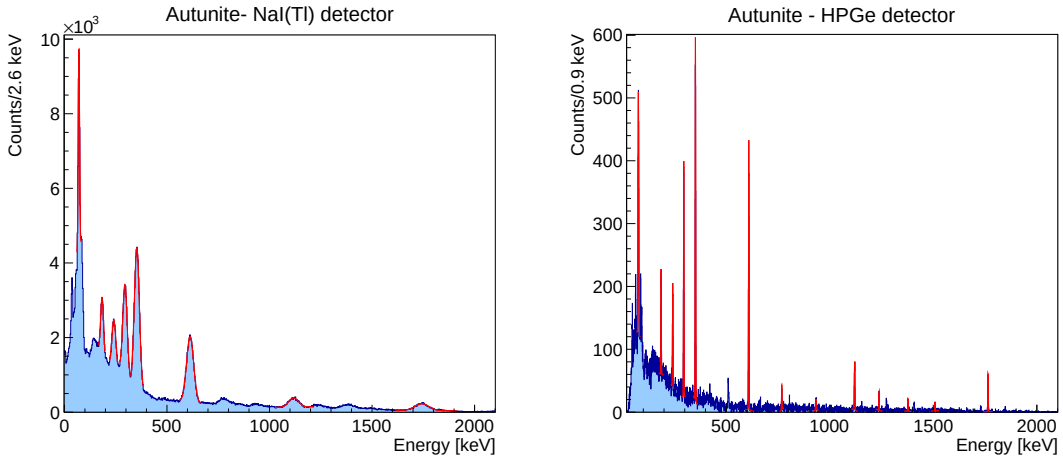

Figure 9: Autunite spectra

NaI(Tl)	
Isotope	Activity [Bq/kg]
^{214}Pb	$(101.3 \pm 0.1) \cdot 10^3$
^{214}Bi	$(94.6 \pm 0.2) \cdot 10^3$
^{226}Ra	$(61.3 \pm 0.2) \cdot 10^3$

Table 15: Autunite sample results for NaI(Tl) detector.

HPGe	
Isotope	Activity [Bq/kg]
^{214}Pb	$(188.2 \pm 0.4) \cdot 10^3$
^{214}Bi	$(50.7 \pm 0.3) \cdot 10^4$
^{226}Ra	$(160.6 \pm 0.6) \cdot 10^3$

Table 16: Autunite sample results for HPGe detector.

5.1 Total activity of analyzed samples

The total activity of the samples in which more than one radionuclide was identified is calculated by summing over all gamma events present in the spectra: results are summarized in Table 17.

Comparing the two detectors, we find a significant discrepancy between the estimated activity. The main explanation is probably the approximate calculation of the distance between source and detectors, and consequently of the geometric efficiency: indeed, the samples have an extended volume, but in the analysis they were always considered to be point-like sources. Additional problems are to be considered for the NaI(Tl), namely the calculation of the solid angle, due to the samples being very close to the detector, and the rough estimation of the efficiency curve, obtained with very few points that did not follow a precise trend.

Detector	Sample	Total activity [Bq/kg]
NaI(Tl)	ZrO_2	$(51.7 \pm 0.3) \cdot 10^3$
HPGe	ZrO_2	$(23.1 \pm 0.1) \cdot 10^4$
NaI(Tl)	Electrodes	$(35.3 \pm 0.6) \cdot 10^4$
HPGe	Electrodes	$(12.8 \pm 0.2) \cdot 10^5$
NaI(Tl)	Porphyry	$(73.2 \pm 0.7) \cdot 10$
HPGe	Porphyry	$(36.5 \pm 0.3) \cdot 10^2$
NaI(Tl)	Autunite	$(257.3 \pm 0.3) \cdot 10^3$
HPGe	Autunite	$(85.5 \pm 0.3) \cdot 10^4$

Table 17: Total results for samples

6 Radon counting

In order to measure the activity of Radon-22 present in an indoor environment, a canister with activated charcoal was weighted and left open in a room. After two days it was retrieved and weighted again. The increase in weight is due to the absorption of water, and from this value it's possible to infer the average humidity in the room during the exposure. The Radon activity per liter of air is computed according to the EPA[6] standards, with the following formula:

$$\mathrm{RN} = \frac{\mathrm{N}}{\mathrm{DF} \cdot \mathrm{E} \cdot \mathrm{CF} \cdot \mathrm{T_s}} \tag{6}$$

- N is the net number of counts obtained from the exposed canister;
- DF is a decay factor which takes into account the part of radon in the canister which can decay before being detected ;
- E is the net number of counts obtained from the calibration canister;
- CF is a calibration factor which takes into account how many liters of air per minutes are filtered from the canister;
- $\mathrm{T_s}$ is the exposure time, expressed in minutes.

The canister has been exposed for about 2 days, so 2880 minutes, and during this time it gained 3.7 g of mass. This value corresponds to a percentage of humidity around 50% and to a calibration factor of CF=0.109 [L/min]. The factor DF has been calculated as:

$$\mathrm{DF} = e^{\frac{\ln(2) \cdot \mathrm{T_s}}{\mathrm{T}_{1/2}}} \tag{7}$$

[6]U.S. Environmental Protection Agency

where $T_{1/2}$ is the Radon decay time taken from LNHB website. The value calculated for DF is:

$$DF = (0.9999 \pm 0.0004)$$

where its error comes from propagation. For what regards the calculation of N and E, first of all, we have subtracted the background taken from a reference empty canister from the spectra of the exposed canister and of the calibration source. The former is used as an air humidity sample, whereas the latter is a calibration sample of Radium-226. Then we have selected the main gamma transitions and we have calculated their area through a gaussian fit (see Tables 18-21): all these areas have been summed to obtain the net number of counts. Counts of the calibrated canister have been normalized to the activity of the ^{226}Ra source taken from the table of radioactive sources present at "Polo Didattico" of Dipartimento di Fisica e Astronomia. We found:

$$N = (27154 \pm 165) \qquad E = (174.6 \pm 0.6)[\text{counts/Bq}]$$

with errors following Poisson distribution. The calibration and air humidity spectra are shown in Figure 10 and Figure 11.

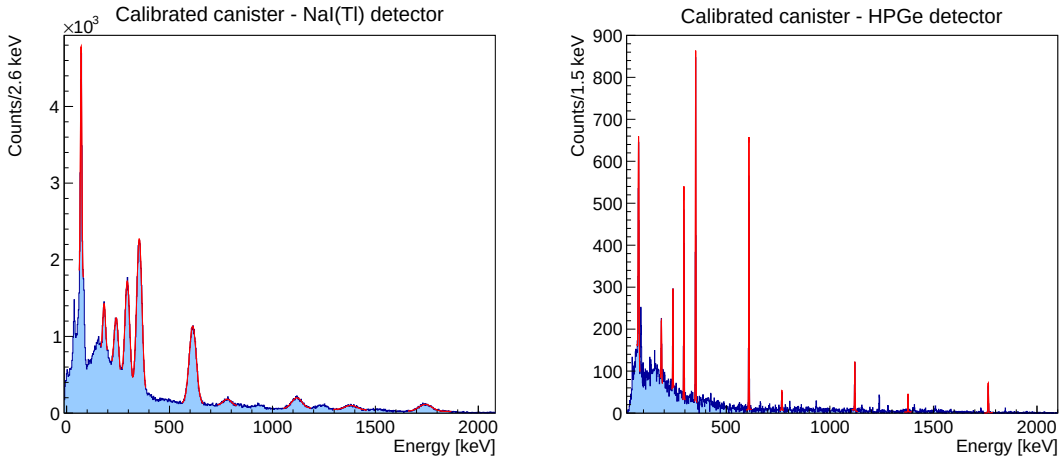

Figure 10: **Calibration sample** spectra.

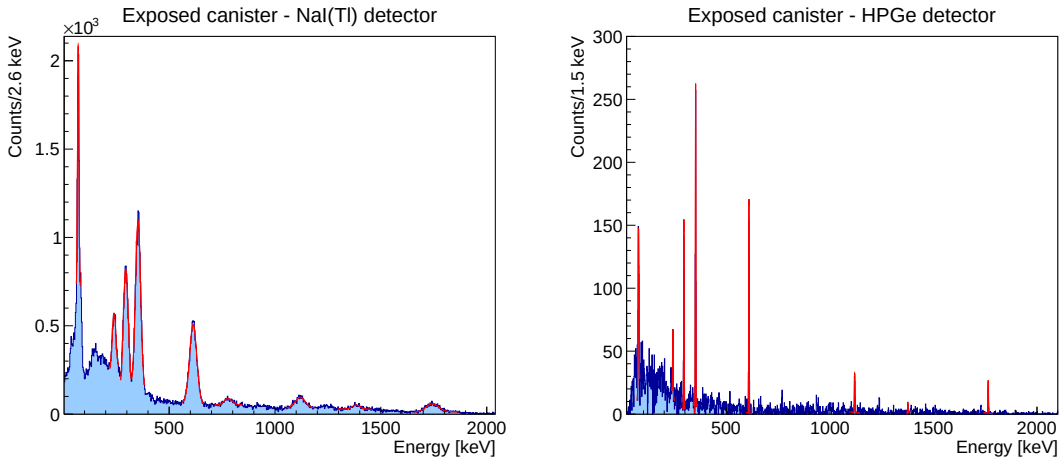

Figure 11: **Exposed sample**, i.e. air humidity, spectra.

Finally we obtain:

$$RN_{NaI} = (698 \pm 2)[\text{Bq/m}^3] \qquad RN_{HPGe} = (424 \pm 4)[\text{Bq/m}^3]$$

The two estimates are not compatible: this might be due to the approximate procedure implemented to obtain our results: nevertheless, we have achieved an acceptable evaluation of the order of magnitude of the radon activity in the air humidity sample. A new decree[7] was signed in 2020 to set limits for radon concentration. It establishes that for existing buildings in working places the maximum tolerable value is 300 Bq/m^3: the values obtained from both the detectors exceed widely this threshold.

Expected Energy [keV]	Branching ratio	Experimental Energy [keV]	N_{peak}
77.1088	10.47(20)	70.48 ± 0.09	$(229.4 \pm 1.5) \cdot 10^2$
186.211(13)	3.555(13)	182.5 ± 0.4	$(132.4 \pm 1.2) \cdot 10^2$
241.997(3)	7.268(22)	241.4 ± 0.6	$(148.6 \pm 1.2) \cdot 10^2$
295.224(2)	18.414(36)	294.9 ± 0.2	$(213.8 \pm 1.5) \cdot 10^2$
351.932(2)	35.60(7)	353.3 ± 0.2	$(299.3 \pm 1.7) \cdot 10^2$
609.312(7)	45.49(19)	612.7 ± 0.2	$(211.2 \pm 1.5) \cdot 10^2$
768.356(10)	1.064(13)	781 ± 2	$(50.1 \pm 0.7) \cdot 10^2$
1120.287(10)	14.91(3)	1118.2 ± 0.9	$(63.2 \pm 0.8) \cdot 10^2$
1377.669(12)	3.968(11)	1381 ± 2	$(42.6 \pm 0.7) \cdot 10^2$
1764.494(14)	15.31(5)	1743 ± 1	$(45.0 \pm 0.7) \cdot 10^2$

Table 18: Measured and expected Energies for **Calibration sample** - NaI(Tl) Detector.

Expected Energy [keV]	Branching ratio	Experimental Energy [keV]	N_{peak}
77.1088	10.47(20)	76.25 ± 0.07	$(27.1 \pm 0.5) \cdot 10^2$
185.720(4)	3.555(13	186.4 ± 0.2	$(9.2 \pm 0.3) \cdot 10^2$
241.997(3)	7.268(22)	242.06 ± 0.09	$(9.0 \pm 0.3) \cdot 10^2$
295.224(2)	18.414(36)	295.11 ± 0.05	$(12.9 \pm 0.4) \cdot 10^2$
351.932(2)	35.60(7)	351.83 ± 0.03	$(19.1 \pm 0.4) \cdot 10^2$
609.312(7)	45.49(19)	609.11 ± 0.04	$(14.2 \pm 0.4) \cdot 10^2$
768.356(10)	4.892(16)	768.2 ± 0.2	$(2.0 \pm 0.1) \cdot 10^2$
1120.287(10)	14.91(3)	1120.2 ± 0.1	$(3.4 \pm 0.2) \cdot 10^2$
1377.669(12)	3.968(11)	1377.5 ± 0.2	$(1.4 \pm 0.1) \cdot 10^2$
1764.494(14)	15.31(5)	1764.5 ± 0.1	$(1.9 \pm 0.1) \cdot 10^2$

Table 19: Measured and expected Energies for **Calibration sample** - HPGe Detector.

Expected Energy [keV]	Branching ratio	Experimental Energy [keV]	N_{peak}
77.1088	10.47(20)	70.4 ± 0.1	$(97 \pm 1.0) \cdot 10^2$
241.997(3)	7.268(22)	239.7 ± 0.6	$(64.5 \pm 0.8) \cdot 10^2$
295.224(2)	18.414(36)	295.0 ± 0.3	$(99 \pm 1) \cdot 10^2$
351.932(2)	35.60(7)	353.3 ± 0.2	$(140 \pm 1) \cdot 10^2$
609.312(7)	45.49(19)	613.4 ± 0.3	$(95 \pm 1) \cdot 10^2$
768.356(10)	4.892(16)	779 ± 2	$(32.5 \pm 0.6) \cdot 10^2$
1120.287(10)	14.91(3)	1118 ± 1	$(30.9 \pm 0.6) \cdot 10^2$
1377.669(12)	3.968(11)	1383 ± 2	$(21.6 \pm 0.5) \cdot 10^2$
1764.494(14)	15.31(5)	1743 ± 1	$(22.8 \pm 0.5) \cdot 10^2$

Table 20: Measured and expected Energies for **Exposed sample** Sample - NaI(Tl) Detector.

Expected Energy [keV]	Branching ratio	Experimental Energy [keV]	N_{peak}
77.1088	10.47(20)	76.3 ± 0.2	$(5.7 \pm 0.2) \cdot 10^2$
241.997(3)	7.268(22)	241.8 ± 0.2	$(2.5 \pm 0.2) \cdot 10^2$
295.224(2)	18.414(36)	295.09 ± 0.08	$(3.6 \pm 0.2) \cdot 10^2$
351.932(2)	35.60(7)	351.65 ± 0.06	$(5.3 \pm 0.2) \cdot 10^2$
609.312(7)	45.49(19)	609.18 ± 0.07	$(3.9 \pm 0.2) \cdot 10^2$
1120.287(10)	14.91(3)	1119.8 ± 0.2	$(1.1 \pm 0.1) \cdot 10^2$
1377.669(12)	3.968(11)	1376.3 ± 0.4	$(3.7 \pm 0.6) \cdot 10$
1764.494(14)	15.31(5)	1764.6 ± 0.2	$(7.2 \pm 0.8) \cdot 10$

Table 21: Measured and expected Energies for **Exposed sample** - HPGe Detector.

7 Conclusions

In order to summarize the obtained results, we can state that the energy calibration results are satisfying for both of the two detectors, in particular the one for the HPGe results highly accurate.
As far as the efficiency is concerned, we obtained:

- **HPGe**: a well-fitting function (i.e. a reliable prediction of the efficiencies values) for high energy, while a phenomenological result for low energies;
- **NaI**: a not reliable fit at any energy.

Some radioactive samples present in the laboratory were analyzed to identify the gamma transitions and determine the activity of the radionuclides of interest (complete results are shown in Table 22): different values were obtained for the two detectors, yet the discrepancy between them could be explained taking into account the approximations introduced in the experimental procedure.
Finally, an indoor Radon measurement was performed: the resulting activity is beyond the legal limit

[7] Decreto legislativo n.101 del 31 luglio 2020 `https://protezioneradon.it/leggi/decreto-legislativo-n-101-del-31-luglio-2020/`

for working environments, but this might be explained considering the fact that the measure was carried out in a small and poorly ventilated room where a high concentration of Radon is expected.

8 Appendix

In the following table we report all data concerning the different samples that we studied. An additional one, i.e. bricks from a military base, was analyzed but not presented in the report. The isotope column indicates the decaying parent nucleus, but the gamma lines identified in the spectra are due to the transition of the daughter nuclei to the ground state.

Detector	Sample	Expected Energy [keV]	Experimental Energy [keV]	Isotope	Photons per 100 disint.	N_{peak}	Activity [Bq/kg]
NaI(Tl)	KCl	1460.822(6)	1452 ± 1	^{40}K	10.55(11)	899 ± 30	$(7.9 \pm 0.3) \cdot 10^3$
HPGe	KCl	1460.822(6)	1460.4 ± 0.1	^{40}K	10.55(11)	111 ± 10	$(5.9 \pm 0.6) \cdot 10^4$
NaI(Tl)	Mushrooms	661.659(3)	667 ± 2	^{137}Cs	94.36(20)	107 ± 10	$(6.6 \pm 0.6) \cdot 10$
Na(Tl)	Bricks	77.1088	78.2 ± 0.4	^{214}Pb	10.47(2)	940 ± 31	$(1.48 \pm 0.05) \cdot 10^3$
Na(Tl)	Bricks	241.997(3)	249 ± 1	^{214}Pb	7.63(2)	274 ± 17	$(11.8 \pm 0.7) \cdot 10^2$
Na(Tl)	Bricks	295.224(2)	300 ± 3	^{214}Pb	18.41(4)	297 ± 17	$(6.0 \pm 0.4) \cdot 10^2$
Na(Tl)	Bricks	351.932(2)	350 ± 4	^{214}Pb	35.60(7)	275 ± 17	$(3.2 \pm 0.2) \cdot 10^2$
HPGe	Bricks	77.1088	82 ± 2	^{214}Pb	10.47(20)	176 ± 13	$(2.6 \pm 0.2) \cdot 10^4$
Na(Tl)	ZrO_2	77.1088	77.9 ± 0.7	^{214}Pb	10.47(20)	$(330 \pm 2) \cdot 10^2$	(318.0 ± 0.6)
Na(Tl)	ZrO_2	186.211(13)	191.7 ± 0.3	^{226}Ra	3.55(19)	$(1257 \pm 4) \cdot 10^2$	$(60.5 \pm 0.2) \cdot 10^2$
Na(Tl)	ZrO_2	241.997(3)	246.3 ± 0.2	^{214}Pb	7.268(22)	$(1719 \pm 4) \cdot 10^2$	$(47.5 \pm 0.1) \cdot 10^2$
Na(Tl)	ZrO_2	295.224(2)	303.7 ± 0.3	^{214}Pb	18.414(36)	$(1766 \pm 4) \cdot 10^2$	$(21.7 \pm 0.4) \cdot 10^2$
Na(Tl)	ZrO_2	351.932(2)	361.4 ± 0.1	^{214}Pb	35.60(7)	$(2135 \pm 5) \cdot 10^2$	$(150.7 \pm 0.3) \cdot 10$
Na(Tl)	ZrO_2	609.312(7)	620.5 ± 0.1	^{214}Bi	45.49(19)	$(1617 \pm 4) \cdot 10^2$	$(124.2 \pm 0.5) \cdot 10$
Na(Tl)	ZrO_2	785.96(9)	784.2 ± 0.9	^{214}Pb	1.064(13)	$(664 \pm 3) \cdot 10^2$	$(25.4 \pm 0.3) \cdot 10^3$
Na(Tl)	ZrO_2	1120.287(10)	1128.0 ± 0.3	^{214}Bi	14.91(3)	$(600 \pm 2) \cdot 10^2$	$(202.7 \pm 0.4) \cdot 10$
Na(Tl)	ZrO_2	1377.669(12)	1392.5 ± 0.7	^{214}Bi	3.968(11)	$(442 \pm 2) \cdot 10^2$	$(63.5 \pm 0.2) \cdot 10^2$
Na(Tl)	ZrO_2	1764.494(14)	1753.1 ± 0.4	^{214}Bi	15.31(5)	$(435 \pm 2) \cdot 10^2$	$(187.8 \pm 0.6) \cdot 10$
HPGe	ZrO_2	77.1088	77.4 ± 0.1	^{214}Pb	10.47(20)	$(63.6 \pm 0.8) \cdot 10^2$	$(264.8 \pm 0.6) \cdot 10$
HPGe	ZrO_2	186.211(13)	186.84 ± 0.07	^{226}Ra	3.55(19)	$(135 \pm 1) \cdot 10^2$	$(31.0 \pm 0.1) \cdot 10^3$
HPGe	ZrO_2	241.997(3)	240.67 ± 0.07	^{214}Pb	7.268(22)	$(160 \pm 1) \cdot 10^2$	$(228.7 \pm 0.7) \cdot 10^2$
HPGe	ZrO_2	295.224(2)	295.71 ± 0.02	^{214}Pb	18.414(36)	$(150 \pm 1) \cdot 10^2$	$(101.0 \pm 0.2) \cdot 10^2$
HPGe	ZrO_2	351.932(2)	352.23 ± 0.02	^{214}Pb	35.60(7)	$(131 \pm 1) \cdot 10^2$	$(53.0 \pm 0.2) \cdot 10^2$
HPGe	ZrO_2	463.002(6)	463.20 ± 0.23	^{228}Ac	4.45(24)	$(26.6 \pm 0.5) \cdot 10^2$	$(10.9 \pm 0.6) \cdot 10^3$
HPGe	ZrO_2	510.74(2)	510.68 ± 0.07	^{208}Tl	22.5(2)	$(30.7 \pm 0.6) \cdot 10^2$	$(27.1 \pm 0.3) \cdot 10^2$
HPGe	ZrO_2	583.108(18)	582.71 ± 0.06	^{208}Tl	85.0(3)	$(32.0 \pm 0.6) \cdot 10^2$	$(8.3 \pm 0.1) \cdot 10^2$
HPGe	ZrO_2	609.312(7)	608.79 ± 0.02	^{214}Bi	45.49(19)	$(105 \pm 1) \cdot 10^2$	$(53.1 \pm 0.3) \cdot 10^2$
HPGe	ZrO_2	768.356(10)	767.34 ± 0.07	^{214}Bi	4.892(16)	$(25.5 \pm 0.5) \cdot 10^2$	$(66.4 \pm 0.8) \cdot 10^3$
HPGe	ZrO_2	911.196(6)	909.69 ± 0.06	^{228}Ac	26.2(8)	$(24.9 \pm 0.5) \cdot 10^2$	$(30.1 \pm 0.9) \cdot 10^2$
HPGe	ZrO_2	934.34(12)	932.55 ± 0.08	^{214}Bi	3.10(1)	$(19.1 \pm 0.4) \cdot 10^2$	$(19.9 \pm 0.6) \cdot 10^3$
HPGe	ZrO_2	968.960(9)	966.5 ± 0.3	^{228}Ac	15.9(5)	$(19.6 \pm 0.4) \cdot 10^2$	$(4.1 \pm 0.1) \cdot 10^3$
HPGe	ZrO_2	1120.287(10)	1118.16 ± 0.04	^{214}Bi	14.91(3)	$(33.3 \pm 0.6) \cdot 10^2$	$(82.7 \pm 0.3) \cdot 10^2$
HPGe	ZrO_2	1238.111(12)	1235.60 ± 0.07	^{214}Bi	5.831(14)	$(18.8 \pm 0.4) \cdot 10^2$	$(128.9 \pm 0.4) \cdot 10^2$
HPGe	ZrO_2	1377.669(12)	1374.69 ± 0.09	^{214}Bi	3.968(11)	$(16.1 \pm 0.4) \cdot 10^2$	$(174.9 \pm 0.5) \cdot 10^2$
HPGe	ZrO_2	1764.494(14)	1760.33 ± 0.04	^{214}Bi	15.31(5)	$(20.7 \pm 0.5) \cdot 10^2$	$(69.9 \pm 0.3) \cdot 10^2$
Na(Tl)	Electrodes		59.5 ± 0.1			$(651 \pm 3) \cdot 10^2$	
Na(Tl)	Electrodes	238.632(2)	245.87 ± 0.06	^{212}Pb	43.6(5)	$(2296 \pm 5) \cdot 10^2$	$(21.2 \pm 0.2) \cdot 10^3$
Na(Tl)	Electrodes	338.320(5)	346.9 ± 0.2	^{228}Ac	11.4(4)	$(1587 \pm 4) \cdot 10^2$	$(6.9 \pm 0.2) \cdot 10^4$
Na(Tl)	Electrodes	463.002(6)	472.3 ± 0.8	^{228}Ac	4.45(24)	$(798 \pm 3) \cdot 10^2$	$(10.7 \pm 0.6) \cdot 10^4$
Na(Tl)	Electrodes	510.74(2)	524.4 ± 0.6	^{208}Tl	22.5(2)	$(1002 \pm 3) \cdot 10^2$	$(28.3 \pm 0.3) \cdot 10^3$
Na(Tl)	Electrodes	583.187(2)	595.9 ± 0.2	^{208}Tl	85.0(3)	$(1543 \pm 4) \cdot 10^2$	$(12.5 \pm 0.1) \cdot 10^3$
Na(Tl)	Electrodes	727.330(9)	739.8 ± 0.7	^{212}Bi	6.65(4)	$(627 \pm 3) \cdot 10^2$	$(74.1 \pm 0.4) \cdot 10^3$
Na(Tl)	Electrodes	911.196(6)	918.7 ± 0.4	^{228}Ac	26.2(8)	$(1181 \pm 3) \cdot 10^2$	$(4.1 \pm 0.1) \cdot 10^4$
HPGe	Electrodes		60.13 ± 0.06			$(30.7 \pm 0.6) \cdot 10^2$	
HPGe	Electrodes	238.632(2)	239.46 ± 0.03	^{212}Pb	43.6(5)	$(71.3 \pm 0.8) \cdot 10^2$	$(33.8 \pm 0.4) \cdot 10^3$
HPGe	Electrodes	300.089	300.7 ± 0.24	^{212}Pb	3.18(14)	$(36.2 \pm 0.6) \cdot 10^2$	$(2.9 \pm 0.1) \cdot 10^5$
HPGe	Electrodes	338.320(5)	338.79 ± 0.06	^{228}Ac	11.4(4)	$(48.5 \pm 0.7) \cdot 10^2$	$(12.0 \pm 0.4) \cdot 10^4$

Detector	Sample	Expected Energy [keV]	Experimental Energy [keV]	Isotope	Photons per 100 disint.	N_{peak}	Activity [Bq/kg]
HPGe	Electrodes	409.460(13)	409.73 ± 0.19	^{228}Ac	2.02(6)	$(12.1 \pm 0.3) \cdot 10^2$	$(20.0 \pm 0.6) \cdot 10^4$
HPGe	Electrodes	463.002(6)	462.9 ± 0.1	^{228}Ac	4.45(24)	$(13.8 \pm 0.4) \cdot 10^2$	$(11.5 \pm 0.6) \cdot 10^4$
HPGe	Electrodes	510.74(2)	510.68 ± 0.05	^{208}Tl	22.5(2)	$(26.3 \pm 0.5) \cdot 10^2$	$(46.9 \pm 0.5) \cdot 10^3$
HPGe	Electrodes	583.187(2)	582.80 ± 0.03	^{208}Tl	85.0(3)	$(39.1 \pm 0.6) \cdot 10^2$	$(20.6 \pm 0.3) \cdot 10^3$
HPGe	Electrodes	727.330(9)	726.47 ± 0.07	^{212}Bi	6.65(4)	$(16.1 \pm 0.4) \cdot 10^2$	$(129.7 \pm 0.8) \cdot 10^3$
HPGe	Electrodes	794.942(14)	793.98 ± 0.09	^{228}Ac	4.31(14)	$(10.8 \pm 0.3) \cdot 10^2$	$(14.5 \pm 0.5) \cdot 10^4$
HPGe	Electrodes	860.53(2)	859.34 ± 0.09	^{208}Tl	12.4(1)	$(7.7 \pm 0.3) \cdot 10^2$	$(38.2 \pm 0.4) \cdot 10^3$
HPGe	Electrodes	911.196(6)	909.77 ± 0.03	^{228}Ac	26.2(8)	$(26.6 \pm 0.5) \cdot 10^2$	$(6.5 \pm 0.2) \cdot 10^4$
HPGe	Electrodes	968.87(10)	966.81 ± 0.07	^{228}Ac	15.9(5)	$(19.0 \pm 0.4) \cdot 10^2$	$(8.0 \pm 0.3) \cdot 10^4$
Na(Tl)	Porphyry	77.1088	77.0 ± 0.3	^{214}Pb	10.47(20)	$(65 \pm 0.8) \cdot 10^2$	120.0 ± 0.3
Na(Tl)	Porphyry	238.632(2)	245.2 ± 0.6	^{212}Pb	43.6(5)	$(67 \pm 0.8) \cdot 10^2$	58.1 ± 0.7
Na(Tl)	Porphyry	338.320(5)	354.7 ± 1.7	^{228}Ac	11.4(4)	$(42 \pm 0.6) \cdot 10^2$	$(17.1 \pm 0.6) \cdot 10$
Na(Tl)	Porphyry	583.187(2)	606.1 ± 1.7	^{208}Tl	85.0(3)	$(35 \pm 0.6) \cdot 10^2$	26.6 ± 0.4
Na(Tl)	Porphyry	1460.822(6)	1454.6 ± 0.7	^{40}K	10.55(11)	$(33 \pm 0.6) \cdot 10^2$	$(35.6 \pm 0.4) \cdot 10$
HPGe	Porphyry	77.1088	76.5 ± 0.3	^{214}Pb	10.47(20)	$(13 \pm 0.4) \cdot 10^2$	$(79.6 \pm 0.3) \cdot 10$
HPGe	Porphyry	238.632(2)	239.9 ± 0.2	^{212}Pb	43.6(5)	$(11 \pm 0.3) \cdot 10^2$	$(36.2 \pm 0.6) \cdot 10$
HPGe	Porphyry	583.187(2)	583.2 ± 0.3	^{208}Tl	85.0(3)	$(3 \pm 0.2) \cdot 10^2$	$(6.3 \pm 0.3) \cdot 10$
HPGe	Porphyry	911.196(6)	910.4 ± 0.3	^{228}Ac	26.2(8)	$(2 \pm 0.1) \cdot 10^2$	$(3.2 \pm 0.1) \cdot 10^2$
HPGe	Porphyry	1460.822(6)	1457.7 ± 0.1	^{40}K	10.55(11)	$(3 \pm 0.2) \cdot 10^2$	$(21.2 \pm 0.3) \cdot 10^2$
Na(Tl)	Autunite	77.1088	70.6 ± 0.1	^{214}Pb	10.47(20)	$(50.4 \pm 0.2) \cdot 10^3$	$(219.5 \pm 0.4) \cdot 10^2$
Na(Tl)	Autunite	186.211(13)	183.7 ± 0.3	^{226}Ra	3.55(19)	$(28.2 \pm 0.2) \cdot 10^3$	$(61.3 \pm 0.2) \cdot 10^3$
Na(Tl)	Autunite	241.997(3)	241.0 ± 0.4	^{214}Pb	7.268(22)	$(29.7 \pm 0.2) \cdot 10^3$	$(37.0 \pm 0.1) \cdot 10^3$
Na(Tl)	Autunite	295.224(2)	295.3 ± 0.2	^{214}Pb	18.414(36)	$(43.0 \pm 0.2) \cdot 10^3$	$(238.2 \pm 0.5) \cdot 10^2$
Na(Tl)	Autunite	351.932(2)	353.2 ± 0.1	^{214}Pb	35.60(7)	$(58.1 \pm 0.2) \cdot 10^3$	$(185.0 \pm 0.5) \cdot 10^2$
Na(Tl)	Autunite	609.312(7)	613.0 ± 0.2	^{214}Bi	45.49(19)	$(39.0 \pm 0.2) \cdot 10^3$	$(135.1 \pm 0.6) \cdot 10^2$
Na(Tl)	Autunite	1120.287(10)	1117.4 ± 0.6	^{214}Bi	14.91(3)	$(15.4 \pm 0.1) \cdot 10^3$	$(60.0 \pm 0.1) \cdot 10^3$
Na(Tl)	Autunite	1764.494(14)	1743.9 ± 0.7	^{214}Bi	15.31(5)	$(10.8 \pm 0.1) \cdot 10^3$	$(210.8 \pm 0.8) \cdot 10^2$
HPGe	Autunite	77.1088	76.35 ± 0.06	^{214}Pb	10.47(20)	$(41.3 \pm 0.6) \cdot 10^2$	$(59.1 \pm 0.1) \cdot 10^3$
HPGe	Autunite	186.211(13)	186.01 ± 0.08	^{226}Ra	3.55(19)	$(20.2 \pm 0.4) \cdot 10^2$	$(160.6 \pm 0.6) \cdot 10^3$
HPGe	Autunite	241.997(3)	241.90 ± 0.07	^{214}Pb	7.268(22)	$(11.8 \pm 0.3) \cdot 10^2$	$(57.9 \pm 0.2) \cdot 10^3$
HPGe	Autunite	295.224(2)	295.13 ± 0.04	^{214}Pb	18.414(36)	$(16.8 \pm 0.4) \cdot 10^2$	$(38.8 \pm 0.2) \cdot 10^3$
HPGe	Autunite	351.932(2)	351.70 ± 0.03	^{214}Pb	35.60(7)	$(23.2 \pm 0.5) \cdot 10^2$	$(32.4 \pm 0.2) \cdot 10^3$
HPGe	Autunite	609.312(7)	609.08 ± 0.03	^{214}Bi	45.49(19)	$(15.5 \pm 0.4) \cdot 10^2$	$(27.0 \pm 0.3) \cdot 10^3$
HPGe	Autunite	768.356(10)	768.4 ± 0.1	^{214}Bi	4.892(16)	$(2.1 \pm 0.1) \cdot 10^2$	$(19.1 \pm 0.2) \cdot 10^4$
HPGe	Autunite	934.34(12)	933.8 ± 0.3	^{214}Bi	3.10(1)	$(1.7 \pm 0.1) \cdot 10^2$	$(6.0 \pm 0.2) \cdot 10^4$
HPGe	Autunite	1120.287(10)	1120.10 ± 0.09	^{214}Bi	14.91(3)	$(3.7 \pm 0.2) \cdot 10^2$	$(31.9 \pm 0.3) \cdot 10^3$
HPGe	Autunite	1238.111(12)	1238.2 ± 0.1	^{214}Bi	5.831(14)	$(1.8 \pm 0.1) \cdot 10^2$	$(42.4 \pm 0.2) \cdot 10^3$
HPGe	Autunite	1377.669(12)	1377.7 ± 0.2	^{214}Bi	3.968(11)	$(1.0 \pm 0.1) \cdot 10^2$	$(38.7 \pm 0.2) \cdot 10^3$
HPGe	Autunite	1509.228(15)	1508.1 ± 0.3	^{214}Bi	2.128(10)	$(1.2 \pm 0.1) \cdot 10^2$	$(89.4 \pm 0.5) \cdot 10^3$
HPGe	Autunite	1764.494(14)	1764.42 ± 0.09	^{214}Bi	15.31(5)	$(2.4 \pm 0.2) \cdot 10^2$	$(27.5 \pm 0.3) \cdot 10^3$

Table 22: Samples data